frontiers in Earth Science

ORIGINAL RESEARCH
published: 21 October 2020
doi: 10.3389/feart.2020.528753

Quantifying Light Dilution in Ultraviolet Spectroscopic Measurements of Volcanic SO_2 Using Dual-Band Modeling

Matthew Varnam[1], Mike Burton[1], Ben Esse[1], Ryunosuke Kazahaya[2], Giuseppe Salerno[3], Tommaso Caltabiano[3] and Martha Ibarra[4]*

[1] Department of Earth and Environmental Sciences, The University of Manchester, Manchester, United Kingdom, [2] Geological Survey of Japan, National Institute of Advanced Industrial Science and Technology, Tsukuba, Japan, [3] Istituto Nazionale di Geofisica e Vulcanologia, Osservatorio Etneo, Catania, Italy, [4] Instituto Nicaragüense de Estudios Territoriales, Frente a Policlínica Oriental, Managua, Nicaragua

High precision and accuracy in volcanic SO_2 emission rate quantification is critical for eruption forecasting and, in combination with in-plume gas ratios, quantifying global volcanic emission inventories. Light dilution, where scattering of ultraviolet light dilutes plume SO_2 absorbance signals, has been recognized for more than 50 years, but is still not routinely corrected for during gas flux quantification. Here we use modeling and empirical observations from Masaya volcano, Nicaragua, to show that light dilution produces: i) underestimates in SO_2 that can reach a factor of 5 and, at low column densities, cause little impact on standard retrieval fit quality, even for heavily diluted spectra; ii) retrieved SO_2 amounts that are capped by a maximum value regardless of the true amount of SO_2, with this maximum amount being reduced as light dilution increases. Global volcanic volatile emission rates may therefore be significantly underestimated. An easily implementable dual-waveband analysis provides a means to detect, and in clear sky conditions, correct dilution effects directly from the spectra, opening a path to more accurate SO_2 quantifications.

Keywords: SO_2 flux, light dilution, volcanic gas, spectroscopy, magmatic degassing, SO_2 emission rate, dual-band modeling, Masaya Volcano

OPEN ACCESS

Edited by:
John Stix,
McGill University, Canada

Reviewed by:
Christoph Kern,
USGS, United States
Patricia Nadeau,
United States Geological Survey, United States

****Correspondence:***
Matthew Varnam
matthew.varnam@manchester.ac.uk

Specialty section:
This article was submitted to Volcanology, a section of the journal Frontiers in Earth Science

Received: *21 January 2020*
Accepted: *22 September 2020*
Published: *21 October 2020*

Citation:
Varnam M, Burton M, Esse B, Kazahaya R, Salerno G, Caltabiano T and Ibarra M (2020) Quantifying Light Dilution in Ultraviolet Spectroscopic Measurements of Volcanic SO_2 Using Dual-Band Modeling. Front. Earth Sci. 8:528753. doi: 10.3389/feart.2020.528753

INTRODUCTION

Emission rates of volcanic gases, and their relative abundances, provide valuable insights into the magma dynamics that drive volcanic activity (e.g., Malinconico Jr, 1979; Sutton et al., 2001; Oppenheimer et al., 2003; Caltabiano et al., 2004). Sulfur dioxide is the most commonly measured of these gases due to its low background atmospheric concentration and strong spectral ultraviolet absorption features (Platt et al., 2018). Combining SO_2 emission rate with volcanic gas ratios produces an estimate of all major plume emissions (e.g., Burton et al., 2000; Aiuppa et al., 2008; Martin et al., 2010; Sawyer et al., 2011). Volcano observatories monitor unrest and attempt to forecast eruptions by integrating such gas measurements with other data streams. Once released, these gases directly impact climate (e.g., Robock, 2000), global volatile cycles (e.g., Wong et al., 2019) and local air quality (e.g., Delmelle et al., 2002), further increasing the importance of accurate quantification.

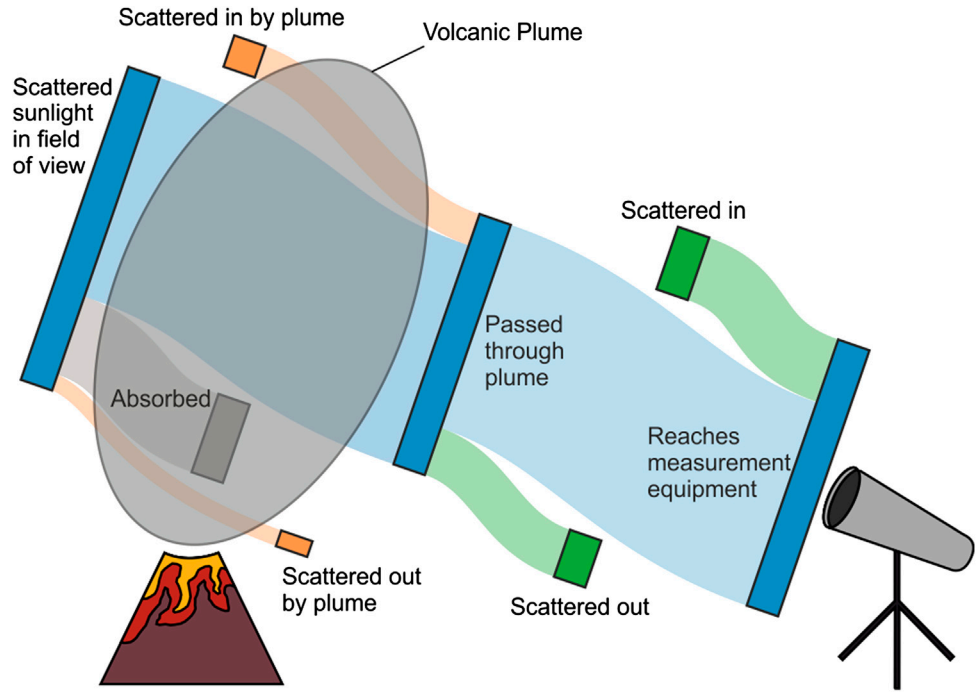

FIGURE 1 | Scattered sunlight (blue) in the field of view of the instrument does not all arrive at the measuring device. Gases in the plume (gray) absorb some of the light. Radiative transfer effects in the plume such as single and multiple scattering by aerosols (orange) also affect how much light reaches the other side. Once out of the plume, photons can be scattered by ambient aerosols and molecules between the plume and the equipment, causing the light dilution effect (green). In general, the impact of light dilution is greater when the distance and opacity of the plume is greater.

SO_2 flux was originally obtained using correlation spectrometers (e.g., Moffat and Millan, 1971; Williams-Jones et al., 2008), but today is more commonly measured using miniature spectrometers (e.g., Galle et al., 2003; Elias et al., 2006). These spectrometers are small, lightweight, and capable of recording moderate-resolution spectra (~0.5–1.0 nm). Spectra are usually analyzed with differential optical absorption spectroscopy (DOAS), retrieving an SO_2 slant column density (SCD) (Platt and Stutz, 2008). Operators traverse beneath or scan across the volcanic plume, creating a cross-section from multiple SCD measurements (e.g., Williams-Jones et al., 2008; Platt et al., 2018). Multiplying a plume SO_2 cross-section by the wind velocity then produces an instantaneous flux. Observatories can also construct SO_2 cross-sections autonomously using zenith pointing spectrometer arrays (Elias et al., 2018) or permanent scanning stations (e.g., Edmonds et al., 2003). Scanning networks are more widespread, including the FLAME network on Sicilian active volcanoes (Salerno et al., 2009a), and the NOVAC network (Galle et al., 2010) which covers 37 volcanoes as of June 2018 (https://novac-community.org/). Researchers have argued that while exact emission rate quantification by scanning networks may be inaccurate, all large changes important for monitoring are observable (e.g., de Moor et al., 2017). Key sources of uncertainty in emission rate quantification are spectroscopic effects, plume velocity, radiative transfer, and in the case of scanners, plume height.

There are two different radiative transfer corrections required, namely for "multiple scattering" and "light dilution" (Bobrowski et al., 2010; Kern et al., 2010). These phenomena are caused by photons interacting with molecules and particles in the air, causing them to scatter elastically (Rayleigh) or inelastically (Raman) (**Figure 1**). Multiple scattering occurs in volcanic plumes where large amounts of ash, water vapor or aerosol are present. With more of these particles, photons passing through a plume have a greater chance of scattering, increasing their travel distance inside the plume relative to the idealized linear path, allowing more absorption to occur. Conversely, the path length could decrease when photons cannot penetrate the center of the plume due to high opacity.

Light dilution arises when photons that have not passed through the plume are scattered into the field of view. While a high aerosol loading of the air between the plume and the detector increases the effect, even a clear atmosphere can cause significant underestimation of the observed SO_2 SCD (Moffat and Millan, 1971; Mori et al., 2006). First-order correction of the dilution relies on its distance-dependence, using simultaneous measurements of the plume from multiple locations (e.g., Bluth et al., 2007; Vogel et al., 2011; Ilanko et al., 2019). Other studies shift their measurements to a higher wavelength range, where both the SO_2 absorption and scattering efficiency are lower, reducing, but not eliminating, the impact (e.g., Bobrowski et al., 2010; Gliß et al., 2015; Fickel and Granados, 2017).

A more thorough correction utilizes full Monte-Carlo photon simulations of the measurement radiative transfer conditions at a single location (Weibring et al., 2002; Kern et al., 2010). These models reveal that dilution dominates over multiple scattering for largely transparent plumes observed at a distance of several kilometers. They, however, do not directly reveal how light dilution affects the spectrum fitting process. Later literature addresses this point (Kern et al., 2012), though the method proposed requires either significant *a priori* knowledge or automatic iteration of lighting conditions, plume geometry and atmospheric properties to correct a spectrum. In practice, this has prevented widespread usage of such models (Arellano et al., 2017). As dilution is the most significant radiative transfer correction required under favorable conditions, a simple, practical method that can detect and quantify the light dilution directly from spectra would be of great benefit.

When light dilution occurs it manifests as a systematic discrepancy in retrieved SO_2 SCDs from different analysis wavelength windows (Mori et al., 2006). The difference between the SCDs retrieved for each waveband, however, is significantly greater than expected from the difference in scattering efficiency alone. In this paper, we also use a dual-waveband approach to identify light dilution occurring, but develop this further using an adapted version of "iFit" (Esse et al., 2020) to model light dilution impacts on the spectra recorded and the retrieved SO_2 SCD. We select the wavebands 306–316 nm (W1) and 312–322 nm (W2) for our analysis. The model allows us to probe the effect light dilution has on a recorded spectrum, explaining the unexpectedly greater difference between retrieved SCDs observed by Mori et al. (2006). We then diagnose and correct light dilution in campaign measurements at Masaya volcano.

MATERIALS AND METHODS

Spectral Fitting

Volcanic SO_2 retrievals typically use traditional implementations of DOAS, such as QDOAS (Danckaert et al., 2012), DOASIS (Kraus, 2006), or custom-made code. The majority of these implementations require a measured spectrum of the sky, clear of any plume (Galle et al., 2003), though some invoke a modeled reference (Salerno et al., 2009b; Hibert et al., 2015; Lübcke et al., 2016). Broadband and narrowband absorption are typically separated, and the narrowband features of the recorded spectrum in a given wavelength range are matched to reference gas spectra. The optical depth of each gas directly retrieves the SCD of that gas.

In this paper, we use an alternative spectral fitting method called "iFit" (short for intensity fitting) for the majority of our analysis, though comparison to QDOAS is available (see **Supplementary Material 1**). iFit fits spectra in intensity space rather than optical depth space. It uses a forward model of a high-resolution (0.01 nm) synthetic spectrum calculated from variable physical parameters. These parameters are iteratively adjusted to fit a pre-processed observed spectrum, which has had the dark spectrum, electronic offset and stray light removed. Full details of this approach can be found elsewhere (Esse et al., 2020), and a coded implementation is available on GitHub (Esse, 2019), but a short summary is provided here.

For each spectrum fit, the iFit forward model starts with a high resolution Fraunhofer spectrum (Chance and Kurucz, 2010). This is similar to other modeled reference techniques (Salerno et al., 2009b), but we do not apply an instrument line shape (ILS) at this stage. Solar light undergoes inelastic scattering in the atmosphere, and this is modeled as a pseudo-absorber, often called the Ring spectrum, which we generate using the QDOAS software (Grainger and Ring, 1962; Danckaert et al., 2012). A background polynomial models other scattering effects. We add absorptions from atmospheric and plume gases, namely SO_2 (Rufus et al., 2003) and O_3 (Gorshelev et al., 2014). Finally, iFit convolves the resulting modeled spectrum with the ILS. This can be summarized with **Eq. 1** below:

$$I(\lambda) = ILS \otimes \left(I_0^*(\lambda) \cdot P(\lambda) \cdot \exp\left[\sum_i [-\sigma_i(\lambda) \cdot a_i]\right]\right) \quad (1)$$

where $I(\lambda)$ is the intensity of the final measured spectrum, λ is the wavelength, $I_0^*(\lambda)$ is the Fraunhofer spectrum, $\sigma_i(\lambda)$ is the absorption cross-section of each absorber i (including the ring pseudo-absorber cross-section and gases), a_i is the SCD of absorber i and $P(\lambda)$ is the third order polynomial. $\otimes$ denotes a convolution. An additional intensity offset option is available to further correct stray light (Esse et al., 2020), but we found subtracting the average intensity between 280 and 290 nm was sufficient in this study.

Light Dilution Theory

Light dilution occurs due to the scattering of photons that have not passed through the plume into the spectrometer field of view. As the distance d between plume and spectrometer increases, there is a greater path over which this scattering can occur. For brevity, we define I_p as the radiant intensity from the plume, such that:

$$I_p(\lambda) = I_0^*(\lambda) \cdot P(\lambda) \cdot \exp\left[\sum_i [-\sigma_i(\lambda) \cdot a_i]\right] \quad (2)$$

Light dilution can be adapted in the final measured spectrum $I(\lambda)$ for a purely scattering atmosphere (Platt and Stutz, 2008; Campion et al., 2015):

$$\begin{aligned} I(\lambda) = ILS \otimes \big(& I_p(\lambda) \cdot \exp[-\sigma_{scat}(\lambda) d] \\ & + I_A(\lambda) \cdot (1 - \exp[-\sigma_{scat}(\lambda) d]) \big) \end{aligned} \quad (3)$$

where I_A is ambient light and σ_{scat} is the scattering coefficient of the atmosphere. For **Eq. 3**, we use the narrow-beam approximation, which requires that the instrument field of view is sufficiently small such that photons scattered out cannot be scattered back in (Platt and Stutz, 2008).

I_A can also be approximated as the intensity of the sky in the viewing direction had it not passed through the plume and been subjected to absorption by SO_2 (Vogel et al., 2011). This allows the formation of **Eq. 4**:

$$I_p(\lambda) = I_A(\lambda) \cdot \exp[-\sigma_{SO_2}(\lambda) \cdot a_{SO_2}] \quad (4)$$

This approximation requires that the scattering sunlight behind the plume has an identical spectral shape to that of the scattering sunlight in front of the plume, and that the plume has no effect on the spectrum other than the absorption of SO_2. These assumptions may be violated, notably for:

- Scattering in a strongly condensing plume or low visibility atmosphere
- Additional wavelength-dependent absorptions in the plume, such as ash.
- Direct sunlight measurements (plume directly between the spectrometer and the Sun)

Assuming **Eq. 4** does hold:

$$I(\lambda) = ILS \otimes \left(I_A(\lambda) \cdot \exp[-\sigma_{SO_2}(\lambda) a_{SO_2}] \cdot \left(\exp[-\sigma_{scat}(\lambda) \cdot d]\right) + I_A(\lambda) \cdot \left(1 - \exp[-\sigma_{scat}(\lambda) \cdot d]\right)\right) \quad (5)$$

The scattering coefficient σ_{scat} depends on optical properties of the atmosphere, such as aerosol concentration, and, crucially, the wavelength of light. If all scattering is due to small gas molecules (Rayleigh), the scattering coefficient is proportional to λ^{-4}. If light encounters many aerosols, however, Mie scattering will occur with a scattering coefficient proportional to around $\lambda^{-1.3}$. We assume a pure Rayleigh scattering atmosphere for our analysis, resulting in an approximate 18% decrease in scattering efficiency as wavelength increases from 306 to 322 nm. Pure Rayleigh scattering represents the ideal scenario of no aerosols in the atmosphere, but using a Mie dependency of $\lambda^{-1.3}$ makes little difference to our modeled results (see **Supplementary Material 2.2**). Note, however, the implications of significant Mie scattering between the plume and instrument, such as greater multiple scattering or backward reflection, would result in deviations from **Eq. 4**.

Light dilution can be expressed as the fraction of light that has not passed through the plume relative to the total intensity before plume absorption is considered.

$$LD(\lambda) = 1 - \exp[-\sigma_{scat}(\lambda) \cdot d] \quad (6)$$

The equation to calculate a diluted spectrum then becomes:

$$I(\lambda) = ILS \otimes \left(I_A(\lambda) \cdot \exp[-\sigma_{SO_2}(\lambda) a_{SO_2}] \cdot (1 - LD(\lambda)) + I_A(\lambda) \cdot LD(\lambda)\right) \quad (7)$$

While we used **Eq. 7** for our model (i.e., light dilution is expressed as a function of wavelength), we report a light dilution factor (LDF) to aid readability of the extent of light dilution occurring. It is specified as the value of LD(λ) at 310 nm, representing the fraction of I_A that is in the second term of the equation (scattered in light) relative to the total I_A.

A calculated literature value of σ_{scat} for pure air (at 0°C and an atmospheric pressure of 1,013.5 mb) at 310 nm is 1.326×10^{-4} m^{-1} (Penndorf, 1957). When this value is placed into **Eq. 6**, LDF will be 0.12 at 1 km and 0.48 at 5 km. This provides a rough estimate of the magnitude of light dilution expected. Also note that due to our formulation in **Eq. 7**, LDF will also vary with linear offsets in light intensity between the two I_A (λ) terms (see **Supplementary Material 2.1**). For example, if light passing through the plume were partially blocked without affecting the spectrum shape, the LDF would increase.

Masaya Field Site

At Masaya volcano, Nicaragua, we collected two sets of measurements: the first using traverses close to the plume for an undiluted measurement as a simple test case of our model, and the other from a static location several kilometers away where light dilution may significantly affect the SO_2 retrieval.

For the undiluted case, we conducted six traverses using an Ocean Optics (now Ocean Insight) FLAME-S-UV-VIS spectrometer on the January 13, 2018. The spectrometer's spectral range is 255–405 nm, with 2,048 pixels and a resolution of ~0.7 at 300 nm. It connected via optical fiber to a collimating telescope, which has a Hoya U330 visible cut filter to remove unwanted wavelengths above 400 nm. Each measurement is a composite spectrum made of 10 coadded individual spectra with an integration time of 500 ms.

The telescope was affixed to a vehicle and aimed vertically upwards. This vehicle drove along a road approximately 5 km away from the vent and 500 m a.s.l., and collected a composite spectrum every 5 s. In total, we recorded 750 of these spectra from 20:47 to 21:54 UTC (local time UTC-6, solar elevation angle 36°–22°). Simultaneous camera measurements observed the plume traveling horizontally after leaving the crater, spreading between the crater floor and ~1,000 m a.s.l., hence the traverse plume to spectrometer distance was small (<1 km).

For a diluted example, we used the same spectrometer attached to a fixed tripod located at the Mirador overview point on the January 15, 2018, aimed obliquely toward the volcano. It observed a point ~300 m above the crater wall and ~700 m downwind of the vent, recording 841 spectra over 70 min from 17:00 to 18:10 UTC (solar elevation angle between 57° and 54°). The plume to spectrometer distance was ~4.8 km, calculated using the intersection of the spectrometer field of view with the volcano to plume-center bearing obtained from simultaneous traverses conducted using a second spectrometer (**Figure 2**).

Modeling the Impact of Light Dilution on Spectra

We produced synthetic spectra with varying SO_2 SCDs and light dilution, so they can be analyzed to observe the impact of light dilution on SO_2 retrieval. First, a synthetic clear spectrum was created that is representative of the lighting conditions using the forward model (**Eq 1**), with optimized parameters of a plume-free spectrum captured on location fitted between 305 and 323 nm. This waveband covers the two smaller fitting windows used, with a 1 nm buffer to avoid edge effects. For our analysis, we chose a spectrum captured at 17:43 UTC on the January 15, 2018 from the Mirador viewpoint, and a spectrum captured at 15:05 UTC on the January 13, 2018 from the traverse measurements, primarily because they are clear from plume contamination. We then produced a suite of

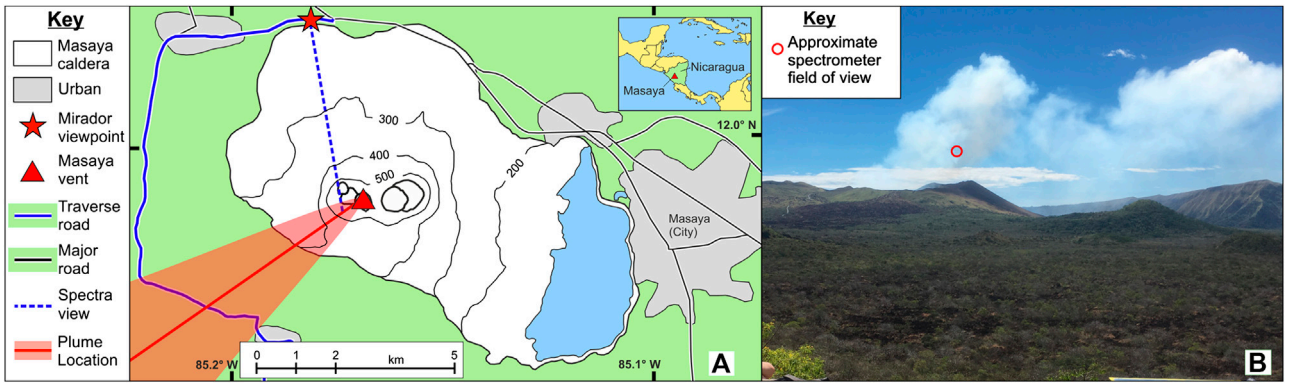

FIGURE 2 | (A) Map of Masaya crater with important measurement locations marked. Traverses were conducted along the Ticuantepe road to the West of the volcano (blue line) and a fixed spectrometer was deployed at the Mirador viewpoint. The plume direction (red line) shown is the average location along the road of the plume center of mass (inset shows the location of Masaya volcano within Nicaragua). **(B)** shows a photograph taken from the Mirador viewpoint with the approximate spectrometer field of view marked.

synthetic spectra using the obtained parameters (**Eq. 7**), but SO_2 SCD is varied in 20 ppm m increments between 0 and 5,000 ppm m and LDF in 0.002 increments between 0 and 0.998. These new spectra were analyzed using the standard iFit approach (**Eq. 1**) without light dilution. Two different wavebands are used, namely 306–316 nm (W1) and 312–322 nm (W2), and the SO_2 SCD retrieved by both was stored (**Figure 3**) in a lookup grid.

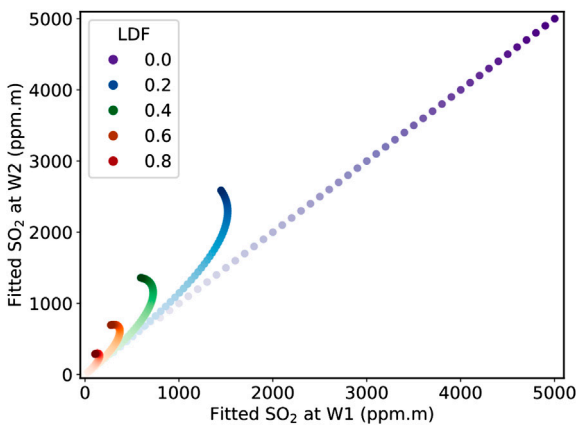

FIGURE 3 | Retrieved SO_2 slant column densities (SCDs) from the analysis of all synthetic spectra generated by varying input SO_2 between 0 and 5,000 ppm m and the light dilution factor (LDF) between 0.0 and 0.8 (here in steps of 0.2 for display purposes). All the synthetic spectra are generated from a single clear spectrum captured from stationary measurements at Masaya volcano and analyzed using the two wavebands W1 (306–316 nm) and W2 (312–322 nm). Darker shading of the points represents increased input SO_2 SCD, with the darkest shade always representing 5,000 ppm m, hence the maximum fitted SCD at both wavebands is less than the input SCD at all LDFs greater than 0. Note how light dilution produces an upper limit on measured gas amounts for LDFs greater than 0.2 in this SO_2 SCD input range.

Correction of the Light Dilution Effect

All Masaya spectra were then analyzed using the standard iFit procedure using the two wavebands W1 and W2. The SO_2 SCDs retrieved at both wavelengths were plotted against each other. Different wavebands should produce different SO_2 SCDs if light dilution is present and identical SCDs if it is not.

We used the uncorrected SCDs retrieved from each spectrum to find the location of the data point on the lookup grid (**Figure 4**). The four bounding points of the lookup table grid are identified, then a best estimate of the LDF and corrected SO_2 SCD is obtained from barycentric interpolation using three of the four points that form a bounding triangle. The error of the LDF and SO_2 was obtained by finding the first lookup LDF and SO_2 grid line that does not contain a point lying within error of the uncorrected measurement SCDs.

Each spectrum was then re-fitted using iFit by including the retrieved LDF in the fitting procedure (using **Eq. 7** inside the iFit forward model). SCDs retrieved at the two wavebands should then be equal, providing the inclusion of the LDF term corrects the residual present in the original fit. This process produces a time-series of corrected SO_2 SCDs, but the error obtained from the lookup table is kept. Results, however, are largely unconstrained for low uncorrected SO_2 SCDs, as the lookup grid is extremely closely spaced close to zero. This means any typical measurement error could cause a large change in retrieved LDF and hence SCD. Therefore, if the uncorrected SO_2 point was within two standard deviations of zero for either SO_2 SCD at W1 or W2, we recorded the retrieved LDF as invalid, and used an average of the last 20 valid LDFs for the refitting instead.

RESULTS

Modeled Spectra

Our simple model explores the effects of light dilution on the spectral fitting process. A modeled LDF of zero results in an exact correspondence between the analysis windows (**Figure 3**). This is

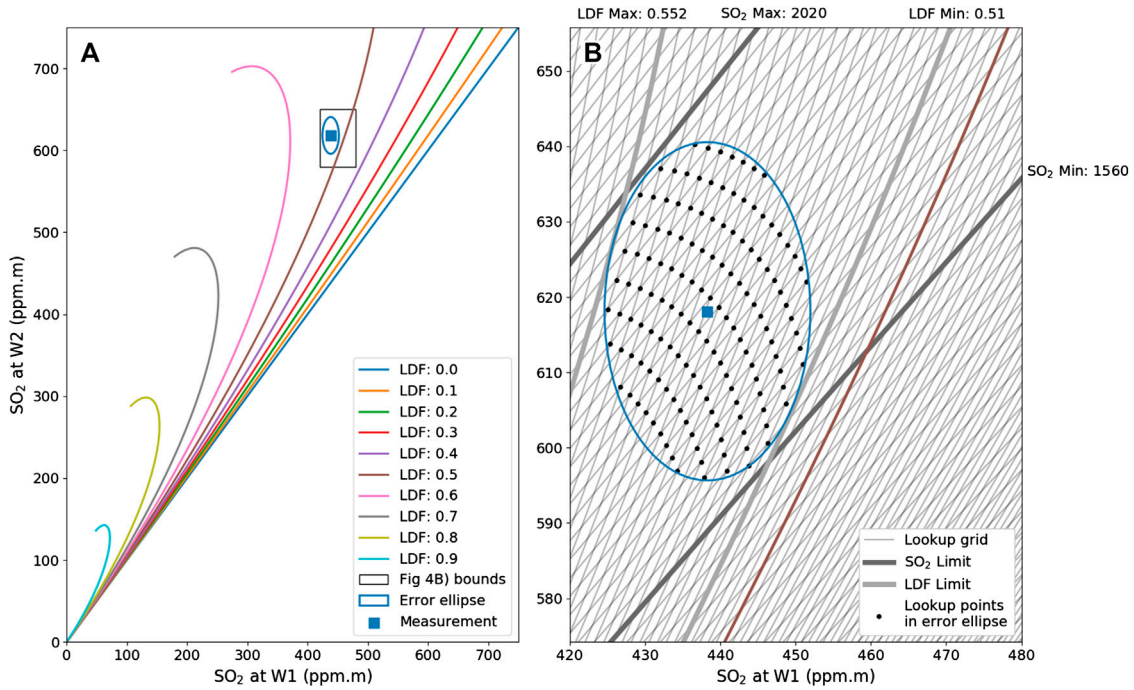

FIGURE 4 | (A) A single measurement of SO_2 (blue square) at W1 (306–316 nm) and W2 (312–322 nm) is shown with a typical fitting error (blue ellipse). It is plotted on a set of light dilution curves spaced with LDFs between 0 and 0.9. The black box highlights the region of the graph for **(B)**. **(B)** Shows the full light dilution lookup table. Here, the SO_2 grid is spaced every 20 ppm m between 0 and 5,000 ppm m, and LDF is spaced every 0.02 between 0 and 0.998. The intersections of the grid that lie in the error ellipse are plotted. An estimate of the SO_2 is made from interpolating the measurement point inside the grid, giving a best estimate of LDF and SO_2. An estimate for the error is provided by finding the first line that does not contain a lookup point inside the error ellipse.

expected, because for zero LDF, the spectrum creation and fitting functions are identical. In both wavelength windows, any light dilution reduces the measured SO_2 SCD, regardless of the original SCD value.

For diluted spectra, as input SO_2 SCD increases there is a greater difference measured between the two retrieved SO_2 SCDs (**Figure 5**), with the 306–316 nm waveband obtaining less SO_2 than the 312–322 nm waveband. A greater LDF also increases the relative difference. This is the large discrepancy in retrieved SO_2 SCD observed between different wavelength windows described by Mori et al. (2006). It arises because absorption is exponential in intensity space (Beer-Lambert Law) while dilution is linear. Where the absorption is stronger, the effect of the exponential is greater, increasing the effect of the linear dilution

Interestingly, at very high SCDs and LDFs, there appears to be an upper limit on observable SO_2 SCD (e.g., with an LDF of 0.4 present, SO_2 SCDs retrieved at 306–316 nm do not exceed 750 ppm m). This would mean standard retrieval at these wavelengths could not increase in their SO_2 reading for the LDF, while producing SCDs that are relatively small, making quantification very inaccurate. In fact, increasing plume SO_2 SCD in these cases can decrease the measured values, potentially leading to large underestimates. This surprising result was also produced in Kern et al. (2012) with their more complex radiative transfer modeling of an SO_2 plume from Kīlauea.

In this fitting of synthetic spectra during the creation of the model, high residuals do not necessarily correspond with high light dilution values. The largest residuals are instead found with greater SO_2 SCD and low non-zero LDFs between 0.1 and 0.2. In contrast, heavily diluted spectra with low SO_2 load may not show detectable above-noise residual in a single analysis window. These residuals are important as a smaller residual is more likely to be below noise, and hence undetectable using standard measurement techniques, but the dilution may still be observable as an offset between the retrieved SO_2 SCDs when dual-wavebands are used.

Light Dilution During Masaya Passive Degassing Measurements

We next tested the model by comparing two sets of measurements captured from two different distances at the same volcano, aiming to replicate and quantify the increase in light dilution with distance. For our undiluted traverse measurements, analysis with both wavebands produced nearly identical results (**Figure 6A**), confirming that there was no detectable light dilution in these measurements.

For our diluted oblique measurements, the spectra do not produce a 1:1 agreement between the analysis windows, with analysis using W1 retrieving considerably lower SO_2 SCDs than W2 (**Figure 6B**). The retrieved uncorrected SO_2 SCDs are consistent with an LDF of between 0.4 and 0.6, but there is considerable variation in the raw data.

We used the lookup tables to obtain an estimate of the LDF and a possible SO_2 range for each spectrum. The raw spectra were

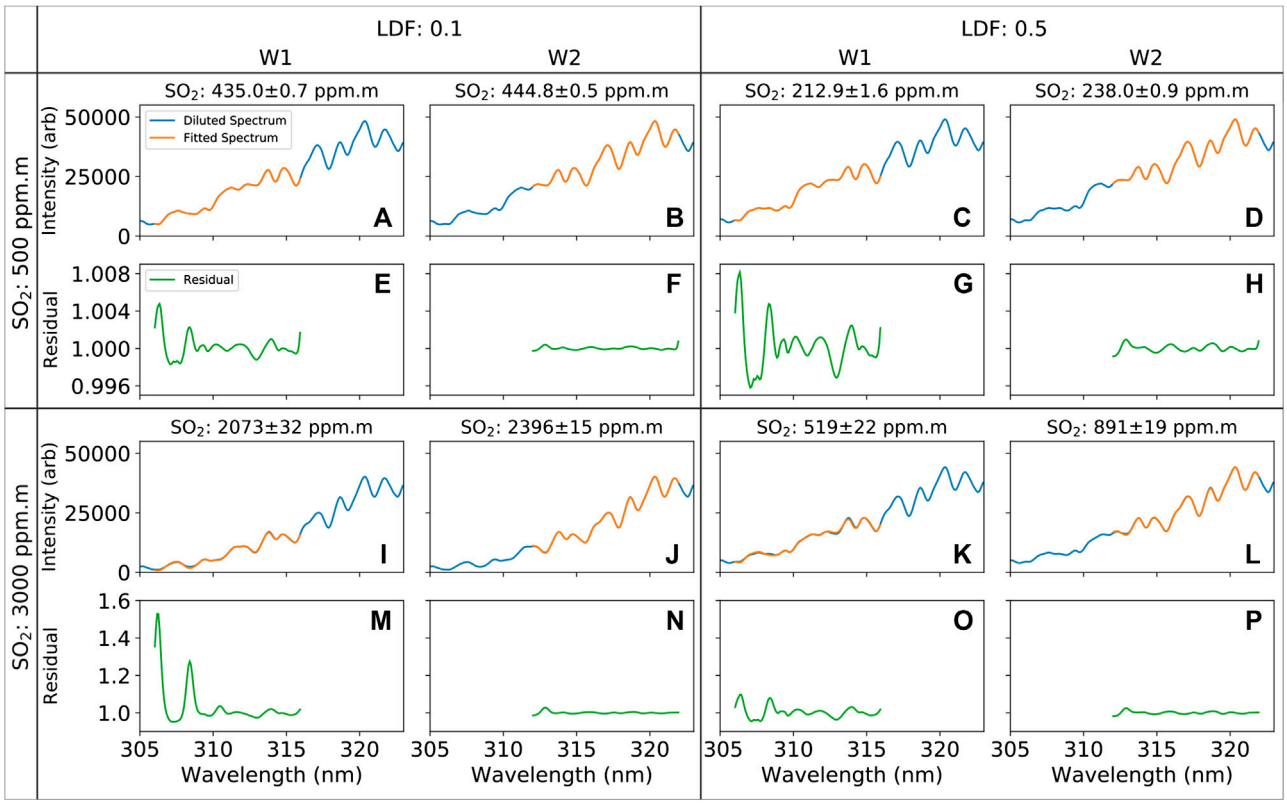

FIGURE 5 | Synthetic spectra (blue) are created from a single Masaya spectrum by varying SO_2 SCD and LDF in the altered forward model (run between 305 and 323 nm). These spectra are then analyzed using the traditional iFit, creating a fitted spectrum (orange). **(A,C,I,K)** show fits for W1 (306–316), while **(B,D,J,L)** show fits for W2 (312–322 nm). The retrieved values are shown above each spectra plot. Residuals of these fits are shown (green), calculated as the synthetic model spectrum divided by the fitted spectrum **(E–H,M–P)**. Note the scale for the residual plots is much larger for the 3,000 than 500 ppm m plots.

then re-fitted using the estimated LDFs. Retrieved SO_2 SCDs using the estimated LDFs were almost identical between the two wavebands, suggesting the correction method has successfully removed light dilution (**Figure 7**). SO_2 SCDs are up to 5 times larger than those of the original data, with the maximum SO_2 retrieved increasing from 600 for W1 and 900 ppm m for W2 to 3,000 ppm m (**Figure 8**). The estimated LDF slightly increases with increasing corrected SO_2 SCD, possibly due to a slight increase in plume opacity from aerosol and other gas species. There are also longer-scale changes in the LDF, possibly due to changing solar position or atmospheric conditions.

At low SO_2 SCDs, however, both corrected SO_2 SCD and LDF are poorly constrained, as at these uncorrected SO_2 amounts the exact LDF has only a small impact on the residual but a dramatic impact on the corrected SO_2 SCD. This is reflected in the large reported error for these measurements. Large unrealistic spikes in corrected SCD at these very low uncorrected SCDs, however, are successfully avoided using the average LDF of the past few measurements.

DISCUSSION

Our dual-waveband approach allows easy detection of light dilution using both intensity and optical depth fitting. It can also provide an estimate of the magnitude of dilution for intensity fitting under clear conditions, offering a means to correct SO_2 quantification. In our examples, we find correction produces a large increase in retrieved SO_2, up to a factor of 5.

Several studies have noted that light dilution increases with the distance between a spectrometer and a volcanic plume (e.g., Moffat and Millan, 1971; Bluth et al., 2007). The effect was initially presumed to be logarithmic with distance, considering transmitted intensity exponentially decays with distance, but our study and others (Kern et al., 2012) show the relationship is more complex at high SO_2 SCDs. Lower wavebands suffer greater underestimation at such SCDs due to the greater SO_2 absorption present, but show greater fitting residuals.

Our model shows fitting using longer wavelengths, e.g., 314–316 nm (Mori et al., 2006), only improves the fit residual, but does not correct the majority of the underestimation resulting from light dilution (**Figure 5**). Previous work has used wavebands around 360–390 nm to avoid scattering issues (e.g., Bobrowski et al., 2010; Gliß et al., 2015), but rough calculations show this would at most halve the scattering coefficient compared to 306 nm, based on the Rayleigh relationship between wavelength and scattering coefficient. Therefore, these spectra likely will still suffer from light dilution while being indistinguishable in appearance from undiluted spectra.

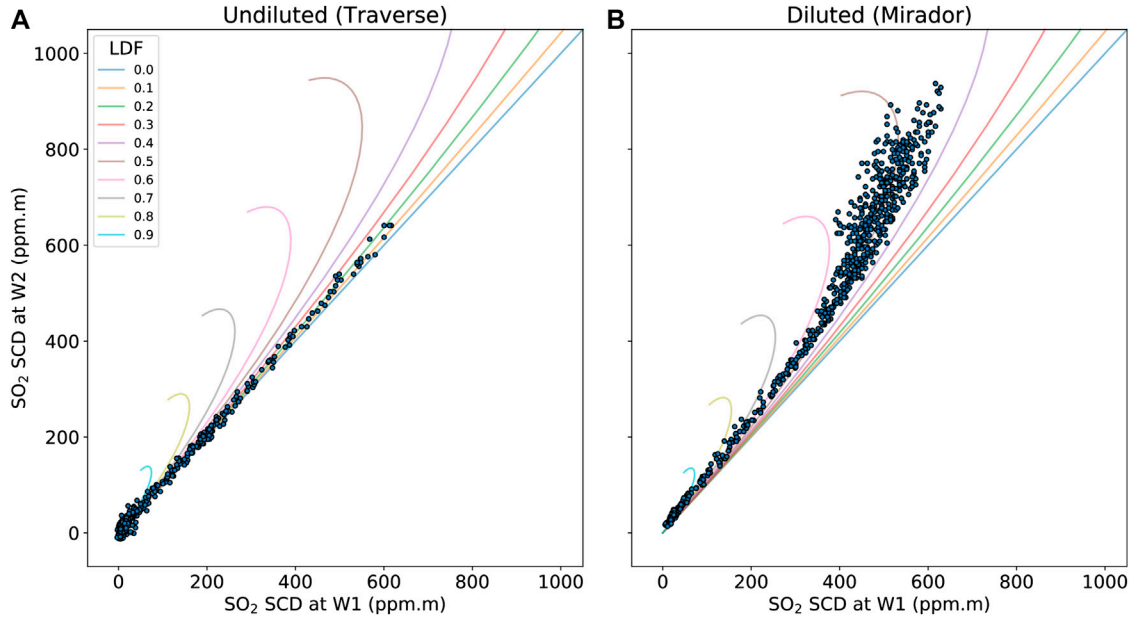

FIGURE 6 | Spectra, taken during the road traverses in panel **(A)**, and from Mirador in panels **(B)**, are analyzed using two different wavebands W1 (306–316 nm) and W2 (312–322 nm). The results are then compared to the model output to estimate the light dilution factor occurring, with LDFs displayed every 0.1 (solid lines).

Strikingly, ignoring light dilution leads to an effective upper limit of quite low SCDs at certain wavelengths. This is because, with traditional analysis, high SCD diluted absorption will yield similar retrieved SCDs to low SCD undiluted absorption. If dilution were systematically ignored during measurements, this limit would mean important changes in emission rate at a volcano could be missed, and eruptive mechanisms misinterpreted. Therefore monitoring techniques may not always be able to detect precursory increases in SO_2 emission rate, defying the commonly held assumption.

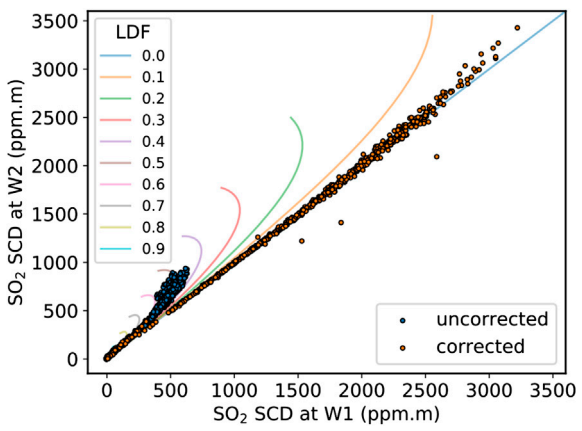

FIGURE 7 | Correction of light dilution in spectra captured from Mirador. The original spectra are analyzed using the W1 (306–316 nm) and W2 (312–322 nm) wavebands, retrieving SO_2 slant column density (blue dots). The light dilution modeled curves (colored lines for LDFs every 0.1) indicate an LDF of between 0.4 and 0.6 is occurring. We then reanalyze the spectra with the LDF determined from the lookup table at both wavebands (orange).

We successfully tested our light dilution model for spectra from Masaya volcano, Nicaragua, showing that at around 5 km from the plume approximately half the light measured at 310 nm had not passed through the plume, consistent with the expected values for clear air. In contrast, we did not detect any dilution for traverses directly beneath the plume. The approach, however, does not include other potential radiative transfer effects. Consequently, we anticipate that our model could perform poorly for an optically thick plume or in a low visibility background atmosphere. Our correction is also poorly constrained for very low SO_2 SCDs, though these points can be identified prior to re-fitting.

Scientists monitoring volcanic SO_2 emissions can readily deploy the dual-waveband approach to detect light dilution. Simply plotting the SCD retrieved in two wavebands is sufficient for detection, as a noticeable curve will be present when dilution is occurring for both DOAS- and iFit-retrieved results. Longer or shorter wavelength wavebands may be needed for very different plume SO_2 SCDs than those presented here, for example during a fissure eruption. If dilution is detected, a number of options are available to scientists. They could reduce the distance between the spectrometer and plume by changing the location of scanners or using an alternative traverse road, but this is not always possible in a mountainous volcanic landscape. Deploying UAV-mounted spectrometers could also help in such landscapes (Stix et al., 2018). Alternatively, our modeling could be used to estimate the dilution occurring under clear conditions. If the more complex Monte-Carlo radiative transfer models were used for correction,

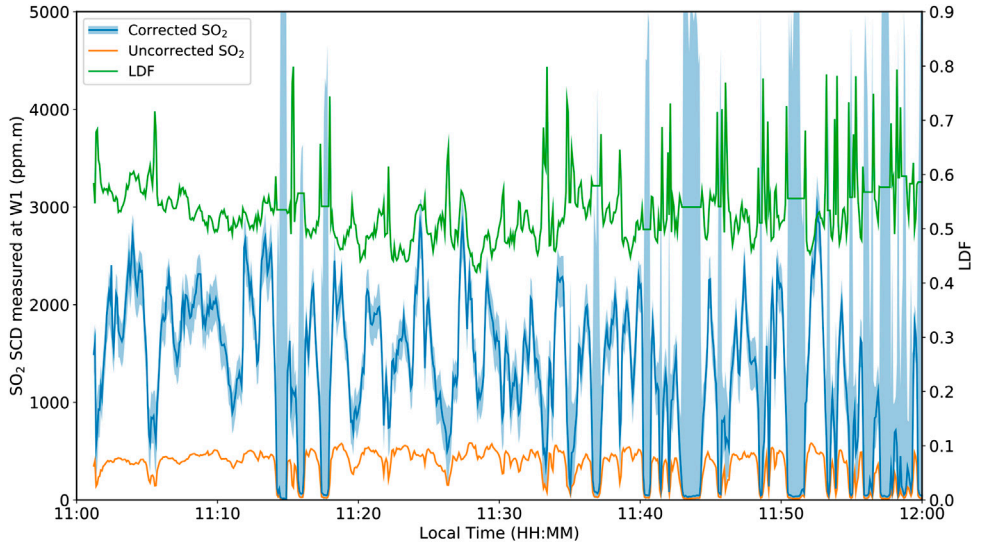

FIGURE 8 | The retrieved SO_2 time series before correction (orange) and after correction (blue). The SO_2 error determined from the lookup table is included as light blue shading. The correction is poorly constrained for low SO_2 SCDs. The light dilution time series is included (green).

our simple modeling could provide additional constraints for their setup.

Light dilution will particularly affect volcanoes with a large distance between their monitoring spectrometers and plume, especially during heightened activity. Many of the volcanoes in the top 50 global emitters of SO_2 (Carn et al., 2016), including Etna (Salerno et al., 2009a), Popocatépetl (Fickel and Granados, 2017), Tungurahua (McCormick et al., 2014; Hidalgo et al., 2015), Nyiragongo and Nyamuragira (Arellano et al., 2017), have traverse roads or deployed scanners at least 1 km below their vent. While volcanoes at high altitudes may be more resilient to the effect due to reduced atmospheric density, a large increase in plume height could still cause significant light dilution to occur. The effect will also be significantly worse if the scanner or road is not situated directly beneath the plume, as the oblique measurement would further increase the spectrometer-plume distance.

We highlight that SO_2 emission rate measured with UV spectroscopy is the primary method used to quantify emissions of other volcanic species, such as CO_2, required for estimates of the total global volcanic CO_2 emission (Burton et al., 2013; Fischer and Aiuppa, 2020); a key parameter in geochemical cycles. Our analysis shows that light dilution can produce large underestimates in SO_2 SCD, and therefore global volcanic SO_2 and CO_2 inventories may also be underestimated.

DATA AVAILABILITY STATEMENT

All datasets generated for this study are included in the manuscript/**Supplementary Material**. The Masaya datasets created for and analyzed during this study are available from Figshare at DOI: 10.6084/m9.figshare.11637462. The base iFit code, and modifications to it detailed in this publication, are available from https://github.com/benjaminesse/iFit.

AUTHOR CONTRIBUTIONS

MV designed code adjustments, analyzed the spectra and drafted the manuscript. BE created the initial iFit code-base. BE, RK, and MI assisted field measurements. MI provided expertise on the activity of Masaya volcano. MB, BE, RK, and GS helped developed the methods used, and all authors reviewed the manuscript.

FUNDING

The work contained in this paper contains work conducted during a PhD study supported by the Natural Environment Research Council (NERC) EAO Doctoral Training Partnership grant number NE/L002469/1 alongside a CASE award from INGV, whose support is gratefully acknowledged.

ACKNOWLEDGMENTS

We would like to thank the staff at INETER for their expertise on Masaya volcano and help with measurements.

SUPPLEMENTARY MATERIAL

The Supplementary Material for this article can be found online at: https://www.frontiersin.org/articles/10.3389/feart.2020.528753/full#supplementary-material

REFERENCES

Aiuppa, A., Giudice, G., Gurrieri, S., Liuzzo, M., Burton, M., Caltabiano, T., et al. (2008). Total volatile flux from Mount Etna. *Geophys. Res. Lett.* 35, L24302. doi:10.1029/2008gl035871

Arellano, S., Yalire, M., Galle, B., Bobrowski, N., Dingwell, A., Johansson, M., et al. (2017). Long-term monitoring of SO_2 quiescent degassing from Nyiragongo's lava lake. *J. Afr. Earth Sci.* 134, 866–873. doi:10.1016/j.jafrearsci.2016.07.002

Bluth, G. J. S., Shannon, J. M., Watson, I. M., Prata, A. J., and Realmuto, V. J. (2007). Development of an ultra-violet digital camera for volcanic SO_2 imaging. *J. Volcanol. Geoth. Res.* 161, 47–56. doi:10.1016/j.jvolgeores.2006.11.004

Bobrowski, N., Kern, C., Platt, U., Hörmann, C., and Wagner, T. (2010). Novel SO_2 spectral evaluation scheme using the 360–390 nm wavelength range. *Atmos. Meas. Tech.* 3, 879–891. doi:10.5194/amt-3-879-2010

Burton, M. R., Oppenheimer, C., Horrocks, L. A., and Francis, P. W. (2000). Remote sensing of CO_2 and H_2O emission rates from Masaya volcano, Nicaragua. *Geology* 28, 915–918. doi:10.1130/0091-7613(2000)28<915:rsocah>2.0.co;2

Burton, M. R., Sawyer, G. M., and Granieri, D. (2013). 11. Deep carbon emissions from volcanoes. *Rev. Mineral. Geochem.* 75, 323–354. doi:10.2138/rmg.2013.75.11

Caltabiano, T., Burton, M., Giammanco, S., Allard, P., Bruno, N., Murè, F., et al. (2004). Volcanic gas emissions from the summit craters and flanks of Mt. Etna, 1987–2000. *Geophys. Mon. Ser.* 143, 111–128. doi:10.1029/143GM08.

Campion, R., Delgado-Granados, H., and Mori, T. (2015). Image-based correction of the light dilution effect for SO_2 camera measurements. *J. Volcanol. Geoth. Res.* 300, 48–57. doi:10.1016/j.jvolgeores.2015.01.004

Carn, S. A., Clarisse, L., and Prata, A. J. (2016). Multi-decadal satellite measurements of global volcanic degassing. *J. Volcanol. Geoth. Res.* 311, 99–134. doi:10.1016/j.jvolgeores.2016.01.002

Chance, K., and Kurucz, R. L. (2010). An improved high-resolution solar reference spectrum for earth's atmosphere measurements in the ultraviolet, visible, and near infrared. *J. Quant. Spectrosc. Radiat. Transf.* 111, 1289–1295. doi:10.1016/j.jqsrt.2010.01.036

Danckaert, T., Fayt, C., Van Roozendael, M., De Smedt, I., Letocart, V., Merlaud, A., et al. (2012). *QDOAS Software user manual*. Belgian Institute for Space Aeronomy (BIRA-IASB). Available at: http://uv-vis.aeronomie.be/software/QDOAS/QDOAS_manual.pdf (Accessed October 7, 2020).

de Moor, J. M., Kern, C., Avard, G., Muller, C., Aiuppa, A., Saballos, A., et al. (2017). A new sulfur and carbon degassing inventory for the southern central American volcanic arc: the importance of accurate time-series data sets and possible tectonic processes responsible for temporal variations in arc-scale volatile emissions. *Geochem. Geophys. Geosyst.* 18, 4437–4468. doi:10.1002/2017gc007141

Delmelle, P., Stix, J., Baxter, P., Garcia-Alvarez, J., and Barquero, J. (2002). Atmospheric dispersion, environmental effects and potential health hazard associated with the low-altitude gas plume of Masaya volcano, Nicaragua. *Bull. Volcanol.* 64, 423–434. doi:10.1007/s00445-002-0221-6

Edmonds, M., Herd, R. A., Galle, B., and Oppenheimer, C. M. (2003). Automated, high time-resolution measurements of SO_2 flux at Soufrière Hills Volcano, Montserrat. *Bull. Volcanol.* 65, 578–586. doi:10.1007/s00445-003-0286-x

Elias, T., Kern, C., Horton, K. A., Sutton, A. J., and Garbeil, H. (2018). Measuring SO_2 emission rates at Kīlauea volcano, Hawaii, using an array of upward-looking UV spectrometers, 2014–2017. *Front. Earth Sci.* 6, 214. doi:10.3389/feart.2018.00214

Elias, T., Sutton, A. J., Oppenheimer, C., Horton, K. A., Garbeil, H., Tsanev, V., et al. (2006). Comparison of COSPEC and two miniature ultraviolet spectrometer systems for SO_2 measurements using scattered sunlight. *Bull. Volcanol.* 68, 313–322. doi:10.1007/s00445-005-0026-5

Esse, B. (2019). iFit (computer software). Available at: https://zenodo.org. (Accessed June 25, 2020).

Esse, B., Burton, M., Varnam, M., Kazahaya, R., and Salerno, G. (2020). iFit: a simple method for measuring volcanic SO_2 without a measured Fraunhofer reference spectrum. *J. Volcanol. Geoth. Res.* 402, 107000. doi:10.1016/j.jvolgeores.2020.107000.

Fickel, M., and Delgado Granados, H. (2017). On the use of different spectral windows in DOAS evaluations: effects on the estimation of SO_2 emission rate and mixing ratios during strong emission of Popocatépetl volcano. *Chem. Geol.* 462, 67–73. doi:10.1016/j.chemgeo.2017.05.001

Fischer, T. P., and Aiuppa, A. (2020). AGU centennial grand challenge: volcanoes and deep carbon global CO_2 emissions from subaerial volcanism—recent progress and future challenges. *Geochem. Geophys. Geosyst.* 21, e2019GC008690. doi:10.1029/2019gc008690

Galle, B., Johansson, M., Rivera, C., Zhang, Y., Kihlman, M., Kern, C., et al. (2010). Network for observation of volcanic and atmospheric change (NOVAC)—a global network for volcanic gas monitoring: network layout and instrument description. *J. Geophys. Res.* 115, D05304. doi:10.1029/2009jd011823

Galle, B., Oppenheimer, C., Geyer, A., McGonigle, A. J. S., Edmonds, M., and Horrocks, L. (2003). A miniaturised ultraviolet spectrometer for remote sensing of SO_2 fluxes: a new tool for volcano surveillance. *J. Volcanol. Geoth. Res.* 119, 241–254. doi:10.1016/s0377-0273(02)00356-6

Gliß, J., Bobrowski, N., Vogel, L., Pöhler, D., and Platt, U. (2015). OClO and BrO observations in the volcanic plume of Mt. Etna—implications on the chemistry of chlorine and bromine species in volcanic plumes. *Atmos. Chem. Phys.* 15, 5659–5681. doi:10.5194/acp-15-5659-2015

Gorshelev, V., Serdyuchenko, A., Weber, M., Chehade, W., and Burrows, J. P. (2014). High spectral resolution ozone absorption cross-sections–part 1: measurements, data analysis and comparison with previous measurements around 293 K. *Atmos. Meas. Tech.* 7, 609–624. doi:10.5194/amt-7-609-2014

Grainger, J. F., and Ring, J. (1962). Anomalous Fraunhofer line profiles. *Nature* 193, 762. doi:10.1038/193762a0

Hibert, C., Mangeney, A., Polacci, M., Muro, A. D., Vergniolle, S., Ferrazzini, V., et al. (2015). Toward continuous quantification of lava extrusion rate: results from the multidisciplinary analysis of the 2 January 2010 eruption of Piton de la Fournaise volcano, La Réunion. *J. Geophys. Res. Solid Earth.* 120, 3026–3047. doi:10.1002/2014jb011769

Hidalgo, S., Battaglia, J., Arellano, S., Steele, A., Bernard, B., Bourquin, J., et al. (2015). SO_2 degassing at Tungurahua volcano (Ecuador) between 2007 and 2013: transition from continuous to episodic activity. *J. Volcanol. Geoth. Res.* 298, 1–14. doi:10.1016/j.jvolgeores.2015.03.022

Ilanko, T., Pering, T., Wilkes, T., Apaza Choquehuayta, F., Kern, C., Díaz Moreno, A., et al. (2019). Degassing at Sabancaya volcano measured by UV cameras and the NOVAC network. *Volcanica* 2, 239–252. doi:10.30909/vol.02.02.239252

Kern, C., Deutschmann, T., Vogel, L., Wöhrbach, M., Wagner, T., and Platt, U. (2010). Radiative transfer corrections for accurate spectroscopic measurements of volcanic gas emissions. *Bull. Volcanol.* 72, 233–247. doi:10.1007/s00445-009-0313-7

Kern, C., Deutschmann, T., Werner, C., Sutton, A. J., Elias, T., and Kelly, P. J. (2012). Improving the accuracy of SO_2 column densities and emission rates obtained from upward-looking UV-spectroscopic measurements of volcanic plumes by taking realistic radiative transfer into account. *J. Geophys. Res.* 117, D20302. doi:10.1029/2012jd017936

Kraus, S. (2006). *DOASIS: a framework design for DOAS*. PhD dissertation. Mannheim, Germany: University of Mannheim.

Lübcke, P., Lampel, J., Arellano, S., Bobrowski, N., Dinger, F., Galle, B., et al. (2016). Retrieval of absolute SO_2 column amounts from scattered-light spectra: implications for the evaluation of data from automated DOAS networks. *Atmos. Meas. Techn.* 9, 5677–5698. doi:10.5194/amt-2016-24

Malinconico, L. L., Jr. (1979). Fluctuations in SO_2 emission during recent eruptions of Etna. *Nature* 278, 43–45. doi:10.1038/278043a0

Martin, R., Sawyer, G., Spampinato, L., Salerno, G., Ramirez, C., Ilyinskaya, E., et al. (2010). A total volatile inventory for Masaya Volcano, Nicaragua. *J. Geophys. Res.* 115, B09215. doi:10.1029/2010jb007480

McCormick, B. T., Herzog, M., Yang, J., Edmonds, M., Mather, T. A., Carn, S. A., et al. (2014). A comparison of satellite- and ground-based measurements of SO_2 emissions from Tungurahua volcano, Ecuador. *J. Geophys. Res. Atmos.* 119, 4264–4285. doi:10.1002/2013jd019771

Moffat, A. J., and Millan, M. M. (1971). The applications of optical correlation techniques to the remote sensing of SO_2 plumes using sky light. *Atmos. Environ.* 5, 677–690. doi:10.1016/0004-6981(71)90125-9

Mori, T., Mori, T., Kazahaya, K., Ohwada, M., Hirabayashi, J. I., and Yoshikawa, S. (2006). Effect of UV scattering on SO_2 emission rate measurements. *Geophys. Res. Lett.* 33, 101029. doi:10.1029/2006gl026285

Oppenheimer, C., Pyle, D. M., and Barclay, J. (2003). *Volcanic degassing*. London: Geological Society of London.

Penndorf, R. (1957). Tables of the refractive index for standard air and the Rayleigh scattering coefficient for the spectral region between 02 and 200 μ and their application to atmospheric optics. *J. Opt. Soc. Am.* 47, 176–182. doi:10.1364/josa.47.000176

Platt, U., Bobrowski, N., and Butz, A. (2018). Ground-based remote sensing and imaging of volcanic gases and quantitative determination of multi-species emission fluxes. *Geosciences* 8, 44. doi:10.3390/geosciences8020044

Platt, U., and Stutz, J. (2008). "Introduction," in *Differential optical absorption spectroscopy: principles and applications*. Berlin, Heidelberg: Springer-Verlag, 1–4.

Robock, A. (2000). Volcanic eruptions and climate. *Rev. Geophys.* 38, 191–219. doi:10.1029/1998rg000054

Rufus, J., Stark, G., Smith, P. L., Pickering, J., and Thorne, A. (2003). High-resolution photoabsorption cross section measurements of SO_2, 2: 220 to 325 nm at 295 K. *J. Geophys. Res.* 108, 5011. doi:10.1029/2002je001931

Salerno, G. G., Burton, M. R., Oppenheimer, C., Caltabiano, T., Randazzo, D., Bruno, N., et al. (2009a). Three-years of SO_2 flux measurements of Mt. Etna using an automated UV scanner array: comparison with conventional traverses and uncertainties in flux retrieval. *J. Volcanol. Geoth. Res.* 183, 76–83. doi:10.1016/j.jvolgeores.2009.02.013

Salerno, G. G., Burton, M. R., Oppenheimer, C., Caltabiano, T., Tsanev, V. I., and Bruno, N. (2009b). Novel retrieval of volcanic SO_2 abundance from ultraviolet spectra. *J. Volcanol. Geoth. Res.* 181, 141–153. doi:10.1016/j.jvolgeores.2009.01.009

Sawyer, G. M., Salerno, G. G., Le Blond, J. S., Martin, R. S., Spampinato, L., Roberts, T. J., et al. (2011). Gas and aerosol emissions from Villarrica volcano, Chile. *J. Volcanol. Geoth. Res.* 203, 62–75. doi:10.1016/j.jvolgeores.2011.04.003

Stix, J., de Moor, J. M., Rüdiger, J., Alan, A., Corrales, E., D'Arcy, F., et al. (2018). Using drones and miniaturized instrumentation to study degassing at Turrialba and Masaya volcanoes, Central America. *J. Geophys. Res.: Solid Earth.* 123, 6501–6520.

Sutton, A. J., Elias, T., Gerlach, T. M., and Stokes, J. B. (2001). Implications for eruptive processes as indicated by sulfur dioxide emissions from Kīlauea Volcano, Hawaii, 1979–1997. *J. Volcanol. Geoth. Res.* 108, 283–302. doi:10.1016/s0377-0273(00)00291-2

Vogel, L., Galle, B., Kern, C., Delgado Granados, H., Conde, V., Norman, P., et al. (2011). Early in-flight detection of SO_2 via differential optical absorption spectroscopy: a feasible aviation safety measure to prevent potential encounters with volcanic plumes. *Atmos. Meas. Techn.* 4, 1785–1804. doi:10.5194/amtd-4-2827-2011

Weibring, P., Swartling, J., Edner, H., Svanberg, S., Caltabiano, T., Condarelli, D., et al. (2002). Optical monitoring of volcanic sulphur dioxide emissions-comparison between four different remote-sensing spectroscopic techniques. *Optic Laser. Eng.* 37, 267–284. doi:10.1016/s0143-8166(01)00084-7

Williams-Jones, G., Stix, J., and Hickson, C. (2008). *The COSPEC cookbook: making SO_2 measurements at active volcanoes*. IAVCEI. Methods in Volcanology, 1. Available at: https://www.researchgate.net/publication/302988478_The_COSPEC_Cookbook_Making_SO2_Measurements_at_Active_Volcanoes

Wong, K., Mason, E., Brune, S., East, M., Edmonds, M., and Zahirovic, S. (2019). Deep carbon cycling over the past 200 million years: a review of fluxes in different tectonic settings. *Front. Earth Sci.* 7, 1–22. doi:10.3389/feart.2019.00263

Conflict of Interest: The authors declare that the research was conducted in the absence of any commercial or financial relationships that could be construed as a potential conflict of interest.